

Interplay of Anisotropy and Disorder in the Doping-Dependent Melting and Glass Transitions of Vortices in $\text{Bi}_2\text{Sr}_2\text{CaCu}_2\text{O}_{8+\delta}$

H. Beidenkopf,^{1,*} T. Verdene,¹ Y. Myasoedov,¹ H. Shtrikman,¹ E. Zeldov,¹ B. Rosenstein,² D. Li,³ and T. Tamegai⁴

¹*Department of Condensed Matter Physics, Weizmann Institute of Science, Rehovot 76100, Israel*

²*Electrophysics Department, National Chia Tung University, Hsinchu 30050, Taiwan, Republic of China*

³*Department of Physics, Peking University, Beijing 100871, China*

⁴*Department of Applied Physics, The University of Tokyo, Hongo, Bunkyo-ku, Tokyo 113-8656, Japan*

(Dated: November 11, 2018)

We study the oxygen doping dependence of the equilibrium first-order melting and second-order glass transitions of vortices in $\text{Bi}_2\text{Sr}_2\text{CaCu}_2\text{O}_{8+\delta}$. Doping affects both anisotropy and disorder. Anisotropy scaling is shown to collapse the melting lines only where thermal fluctuations are dominant. Yet, in the region where disorder breaks that scaling, the glass lines are still collapsed. A quantitative fit to melting and replica symmetry breaking lines of a 2D Ginzburg-Landau model further reveals that disorder amplitude weakens with doping, but to a lesser degree than thermal fluctuations, enhancing the relative role of disorder.

PACS numbers: 74.25.Qt, 74.25.Dw, 74.72.Hs, 64.70.Pf

Elasticity, thermal energy, disorder, and inter-layer coupling are some of the closely competing energy scales in the intricate $H - T$ phase diagram of the vortex matter in the layered high temperature superconductor $\text{Bi}_2\text{Sr}_2\text{CaCu}_2\text{O}_{8+\delta}$ (BSCCO) [1, 2, 3, 4, 5, 6]. The low-temperature part of the equilibrium phase diagram of BSCCO was recently made accessible to experiment by vortex shaking [7, 8, 9]. It unveiled a first-order (FO) inverse melting line, which continues the thermal melting line from high temperatures [8] separating low-field ordered phases from high-field amorphous ones. A second-order (SO) transition line, at which low-temperature glassy phases get thermally depinned, was subsequently reported [9]. In this letter we study the oxygen doping dependence of these transition lines. We show that the SO line scales with material anisotropy even where the FO line does not, and that effective disorder weakens with doping, but gains relative dominance over thermal fluctuations.

We present measurements of optimally doped (OPD), slightly over doped (SOD), over doped (OVD) and highly over doped (HOD) BSCCO crystals [10, 11] with critical temperatures $T_c = 92, 90, 88.5$ and 86 K, respectively, corresponding to hole concentrations of $0.171, 0.180, 0.184$ and 0.190 [12]. Various crystal geometries were studied with typical sizes of $\sim 300 \times 300 \times 40 \mu\text{m}^3$. They were mounted on $10 \times 10 \mu\text{m}^2$ Hall sensor arrays, fabricated in a GaAs/AlGaAs heterostructure. At low temperatures we utilized a 350 Oe in-plane ac shaking field of 10 Hz to relax the pancake vortices towards their equilibrium configuration [7, 8, 9]. Conjugating local probes with shaking yielded the equilibrium reversible magnetization of the samples.

Figure 1 shows the local induction, $B(H, T)$, measured in the SOD sample by sweeping the temperature, T , at a constant out-of-plane field, H , in presence of an in-plane shaking field. A linear term $\alpha_H T + \beta_H$ was subtracted

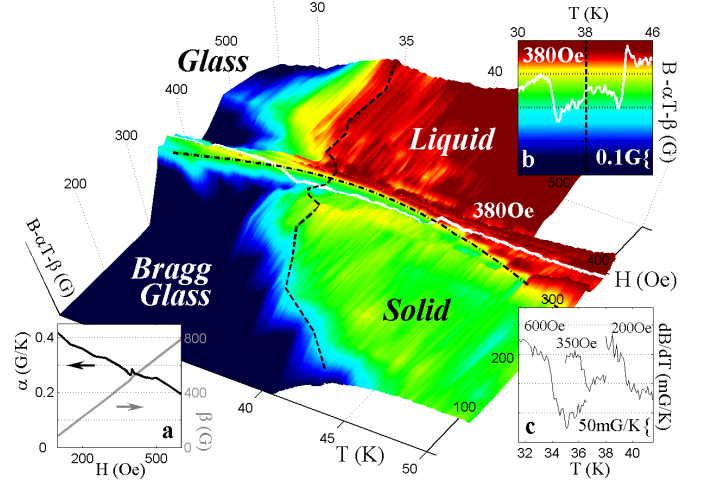


FIG. 1: (color online) The local induction shows FO (dashed-dotted) and SO (dashed) transition lines in the $H - T$ phase diagram. The induction in the high-temperature depinned liquid and solid phases was artificially flattened by a linear subtraction $\alpha_H T + \beta_H$ (hence the constant color). The low-temperature BrG and glassy phases have thus a finite positive slope. (a) Values of α_H and β_H used. (b) FO-SO-FO transition sequence at a 380 Oe temperature sweep on the background of the colorbar. (c) Discontinuous steps in dB/dT , manifesting the SO nature of the transition.

from each temperature sweep (Fig. 1a) to flatten the originally increasing ($\alpha_H > 0$) local induction. As a result, the FO and SO singular behavior can be readily traced throughout the $H - T$ phase diagram.

The FO melting transition is manifested by a discontinuous step in the magnetization along the dashed-dotted line in Fig. 1. It separates the high-field amorphous glass and liquid phases from the low-field quasi-long-range-ordered Bragg glass (BrG) [5, 13]. The melting line becomes nonmonotonic at a certain temperature [8, 9]. Its

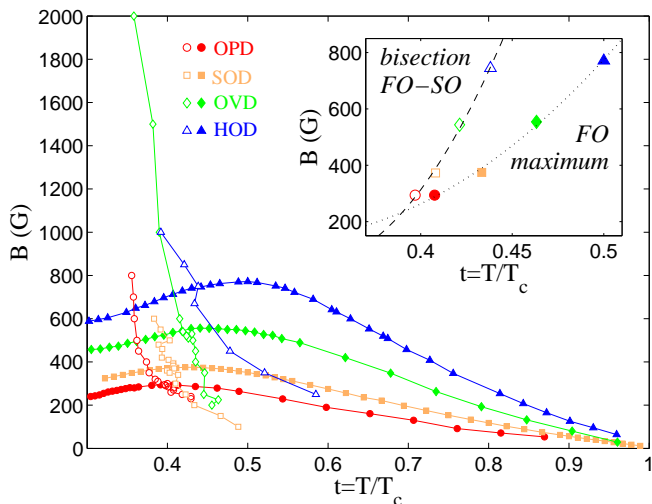


FIG. 2: (color online) FO and SO transition lines (solid and open symbols, respectively) measured with OPD (○), SOD(□), OVD (◇) and HOD (△) samples. The inset shows the doping dependence of the maximum of the FO line and its bisection with the SO line. Dotted and dashed lines are second-degree polynomial fits.

inverse-melting part is believed to be an order-disorder transition, induced mainly by quenched disorder and not by thermal fluctuations [1, 2, 3, 4, 5, 14, 15, 16].

The SO phase transition is manifested by a break in the slope of the magnetization at T_g , marked in Fig. 1 by the dashed line. It separates the fully flattened high-temperature magnetization ($dB/dT|_{T>T_g} - \alpha \approx 0$) of constant color from a low-temperature region of nonzero slope ($dB/dT|_{T<T_g} - \alpha > 0$), whose color varies with temperature. The nonanalyticity at T_g is demonstrated in Fig. 1c, which shows ~ 40 mG/K steps in dB/dT for temperature sweeps lying below as well as above the FO line. The location of the SO line above melting resembles earlier dynamic irreversibility measurements [17, 18, 19, 20, 21] and theoretical models of a glass transition [1, 2, 3, 4, 5, 22, 23, 24]. Few dynamic measurements found a similar line of thermal depinning below melting [9, 25, 26, 27, 28, 29, 30], which separates the BrG phase below it from a thermally depinned solid, whose detailed characteristics are not yet certain.

We mapped three more samples of various doping levels that yielded the $B-T$ phase diagram plotted in Fig. 2. The melting line shifts as a whole to higher fields with doping due to the decrease in anisotropy, which implies stronger inter-layer coupling and higher stiffness of the pancake vortex stacks [10, 30, 31, 32]. As the FO line shifts to higher fields, its maximum shifts towards increasingly higher temperatures (Fig. 2 inset). Identifying these maxima with the crossover from disorder to thermally dominated behavior [1, 2, 3, 4, 5] may suggest that doping enhances disorder. The SO transition line also shifts upwards, further signifying that disorder

is enhanced with doping. However, we will show below that this conclusion is inaccurate. Moreover, arguing naively that the balance between characteristic energies constrains the SO line to bisect the FO one at its maximum [1] is also too simplistic. The inset of Fig. 2 clearly shows that in over-doped samples the bisection point resides below the FO maximum temperature (the overlap of the two in the OPD sample is apparently accidental). Therefore, a naive description of thermal depinning cannot account for both the SO line and the FO maximum behavior (for instance, the latter is directly affected also by elasticity) [2, 3, 4].

We now present a quantitative scaling analysis of the doping dependence, parameterized by the sample anisotropy ratio $\varepsilon^2 = m_{ab}/m_c$ (m_i is the electronic effective mass in the i th direction). For high- κ superconductors, such as BSCCO, the Ginzburg-Landau (GL) free energy functional can be recast into an isotropic ($\varepsilon = 1$) form by rescaling its parameters [33]. We focus on one such transformation [34] that rescales space, magnetic induction, the penetration depth λ_0 and the coherence length ξ_0 . Models for high-temperature melting are usually independent of ξ_0 , and find λ_0 to enter with some model-dependent power as a proportionality factor. For definiteness we resort to a specific model [6, 35] for a FO evaporation line with no disorder from vortex solid to pancake gas $B_E(t) \propto (\varepsilon^2/\lambda_0^2 d)(1-t^2)/t$, where $t = T/T_c$ and d is the inter-plane separation. The scaling transformation [34] indeed renders $B_E(t)$ isotropic.

Figure 3 shows the rescaled FO and SO lines. The high-temperature parts of the FO lines are perfectly collapsed by dividing their induction axes by a constant [30]. $B_E(t)$ (dashed-dotted line) fits the collapsed melting lines precisely, asserting that the multiplicands in this procedure are $(\varepsilon_o/\varepsilon)^2$, normalized by the OPD $\varepsilon_o^{-1} \approx 500$ [36]. Anisotropy scaling collapses the data down to $t_{th} \approx 0.58$. Below t_{th} , which appears to be independent of anisotropy, the rescaled FO lines disperse again, and the fit to $B_E(t)$ breaks. The flattening of the FO line towards an inverse-melting behavior results from quenched disorder, which gains dominance with decreasing temperatures [1]. Accordingly, above t_{th} the FO transition is purely thermally-induced, and completely unaffected by disorder [14]. Just below t_{th} disorder becomes a relevant, though not yet a dominant, energy scale.

This counterparts the extremely low-temperature behavior, where thermal energy becomes negligible relative to pinning, resulting in a flat temperature-independent behavior of the FO lines [1]. Indeed the FO lines in Fig. 3 tend to flatten towards their ends, below which 350 Oe - 10 Hz shaking is insufficient for detecting a reversible melting step. We thus conjectured a similar doping-independent threshold temperature $t_d \approx 0.25$, below which thermal energy becomes irrelevant. We fitted the low-temperature order-disorder lines by a leading order expansion $B_{OD}(t \gtrsim t_d) \sim B_{OD}(t_d) + \Lambda(t-t_d)^2$, which

agrees very well with measurement. We can, therefore, estimate $B_{\text{OD}}(t_d)$, at which elasticity is balanced solely by the disordering potential. It increases monotonically with doping (inset of Fig. 3), stating that with reducing anisotropy elasticity gains dominance also over disorder.

Yet, the most remarkable outcome of the anisotropy scaling shown in Fig. 3 is the simultaneous collapse of the SO transition lines (with zero freedom). The SO lines reside in a temperature region where anisotropy scaling of the melting lines fails due to effects of disorder. Still, the same scaling transformation somehow succeeds in rendering the glass-transition isotropic, even though this transition is believed to be intimately related with the competition between disorder and thermal fluctuations.

To gain deeper understanding of the low-temperature behavior we fit the measured transition lines to those predicted by a recent calculation [37], which gives access to the doping dependence of the model's free parameters. It incorporates thermal, disordering and elastic energies to yield bisecting FO and SO lines. The pancake vortex system is modeled by the 2D GL theory. We interpret this single layer model as the outcome of an integration of all other layers out of a complete 3D theory, resulting in an effective 2D model whose renormalized coefficients may still depend on anisotropy ε of a 3D mass tensor.

The free energy functional is averaged over gaussian disorder in the coefficients of the quadratic and quartic terms using the replica method. Taking the lowest-Landau-level (LLL) approximation yields for the replicated partition function

$$\overline{\mathcal{Z}^n} = \int_{\Psi_1 \dots \Psi_n} \exp \left(- \sum_a G_0(\Psi_a) + \sum_{a,b} \tilde{R} |\Psi_a|^2 |\Psi_b|^2 \right),$$

$$G_0(\Psi) = \int \frac{d^2x}{4\pi} \left(a_T |\Psi|^2 + \frac{|\Psi|^4}{2} + \frac{\kappa^2 (b-h)^2}{\pi \sqrt{2Gi}bt} \right),$$

where $\tilde{R} = a_T^2 b R / 32\pi^2$, R is the disorder amplitude in the coefficient of the quadratic LLL term, $b = B / \tilde{H}_{c2}$, $a_T = (b+t-1) / (2\pi^2 b^2 t^2 Gi)^{1/4}$ is the LLL parameter, Gi is the effective Ginzburg number that generally scales thermal fluctuations, and κ is the GL parameter. Randomness in the coefficient of the quartic LLL term, although crucial for obtaining the non-analyticity of SO, has negligible effect on the locus of the transition lines, and is therefore neglected in the present context.

The FO line is calculated by equating the energies of the homogeneous and crystalline states under the influence of disorder in gaussian approximation. This extends beyond the earlier calculation, which treated disorder perturbatively [38]. The glass line is found from the stability analysis of the replica symmetric solution. The replica symmetry breaking (RSB) is continuous. The corresponding Parisi function describing the hierarchical structure of the glassy state and its detailed derivation can be found in Ref. [37].

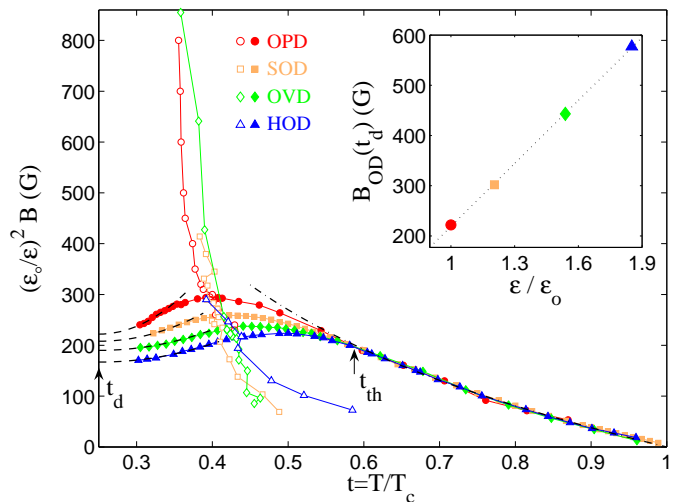


FIG. 3: (color online) Data collapse of the over-doped high-temperature ($t > t_{\text{th}}$) FO lines (solid symbols) onto the OPD line, which also collapses the SO lines (open symbols). The fit to $B_E(t)$ (dashed-dotted) sets the anisotropy ratios $\varepsilon/\varepsilon_0$ to 1, 1.20, 1.54 and 1.85 for the OPD (\circ), SOD (\square), OVD (\diamond) and HOD (\triangle) samples, respectively. The inset shows the linear dependence of the characteristic $B_{\text{OD}}(t_d)$ on $\varepsilon/\varepsilon_0$ (dotted line).

The model's free parameters are R , Gi , \tilde{T}_c , and $\tilde{H}_{c2} = T_c \frac{d\tilde{H}_{c2}}{dT} |_{T_c}$. However, due to a hidden symmetry, given by Gi/\tilde{H}_{c2}^2 and Gi/R^2 , the theory effectively has only three independent fitting parameters. We therefore fixed $\tilde{H}_{c2} = 100T$, for simplicity, consistent with our limited range of hole concentrations [12]. Figure 4 presents two fitting strategies motivated by different physical behaviors. The first (thick lines) is optimized to fit the collapsed parts of the phase diagram - SO lines and FO ones for $t > t_{\text{th}}$. Interestingly, this set simultaneously provides a collapsed FO line also for $t < t_{\text{th}}$. This results from the above symmetry of the model in which Gi and ε take the same role, defining a relation $R \propto \sqrt{Gi}$ along which the calculated phase diagram remains unchanged under anisotropy rescaling. The thick lines in Fig.4 insets show the resulting parameters $Gi = 3.91(\varepsilon_0/\varepsilon - 0.37)^2$ and $R = 1.54(\varepsilon_0/\varepsilon - 0.37)$. The departure of the calculated FO line (thick dashed) from the measured ones below t_{th} may indicate that theory lacks a symmetry-breaking mechanism once anisotropy scaling breaks in experiment.

An alternative fit (thin lines), faithful to the complete FO lines, dictates the slightly different set of values $Gi = 4.77(\varepsilon_0/\varepsilon - 0.38)^2$, $R = 0.75(\varepsilon_0/\varepsilon - 0.2)$ (insets, thin lines). The excellent fit of the FO lines (dashed) suggests that the effective 2D model still captures the essential physics involved. Its validity should break down at very low temperatures, where indeed it misses the flattening of the FO lines as t_d is approached, and close to T_c due to critical fluctuations, which may explain the 10% overestimate in the fitted bare \tilde{T}_c values [39]. Substitut-

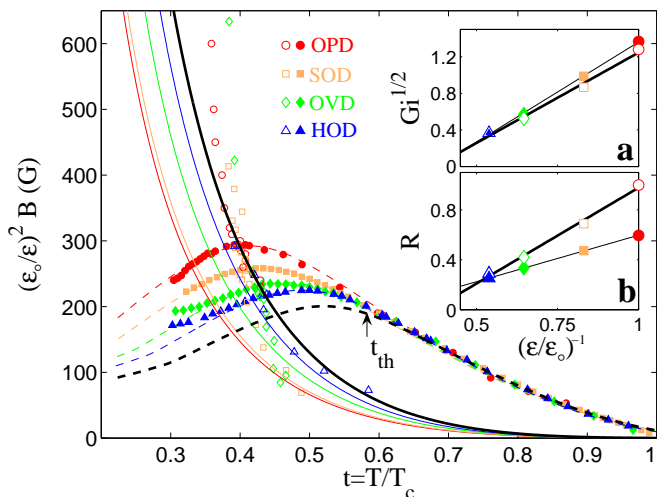


FIG. 4: (color online) Fits of FO (dashed) and SO (solid) lines of the LLL 2D GL model with $\tilde{H}_{c2} = 100$ T, $\tilde{T}_c = 103, 101, 98$ and 95 K for the OPD (\circ), SOD (\square), OVD (\diamond) and HOD (\triangle) samples, respectively. The values of Gi (a) and R (b) were fixed either by fitting the SO lines and FO ones above t_{th} (thick lines) or by fitting the full FO lines (thin lines).

ing this set of values in the calculation of the RSB lines (solid) with zero freedom also produces a good fit that improves with doping, but misses the anisotropy rescaling of the measured SO lines. Nevertheless, the discrepancy between the two sets of values of the different fitting strategies is small, and vanishes in the high doping limit.

In Fig. 4a the reduced dominance of thermal fluctuations with doping is clearly captured by the decrease in Gi . Its dependence on anisotropy is closer to the 3D $1/\varepsilon^2$ than to the 2D ε -independent behavior. Remarkably, the disorder amplitude in Fig. 4b also decreases with doping. This contrasts the result of Ref. [40], which found that oxygen addition increases the defects concentration. The apparent contradiction is resolved by noting that the disorder amplitude is affected also by the anisotropy dependence of the effective pinning potential, which decreases with doping as the vortex stacks get stiffer. The overall decrease of R suggests that the latter mechanism is dominant, not the rising defect concentration.

Last, while both Gi and R decrease with doping, Gi has a stronger dependence on anisotropy. This clarifies the true mechanism that shifts the maximum of the FO line and its bisection with the SO line towards higher temperatures with doping (Fig. 2). Although the magnitude of the disorder amplitude decreases with increased doping, disorder still gains *relative* dominance over thermal fluctuations, which decrease faster with ε .

In summary, ε^2 scaling accounts for the reduced anisotropy of BSCCO samples with doping down to t_{th} . Below t_{th} , where disorder becomes relevant, ε^2 scaling still collapses the SO lines. From the quantitative agreement with the LLL 2D GL model we deduce that disorder

and thermal-fluctuations weaken relative to elasticity with increased doping, which shifts the FO line towards higher fields. Disorder still gains relative dominance over thermal fluctuations, which concurrently shifts the maximum of the FO line and its bisection with the SO line towards higher temperatures.

We thank V.M. Vinokur, and G.P. Mikitik for stimulating discussions. This work was supported by the Israel Science Foundation Center of Excellence, by the German-Israeli Foundation G.I.F., by Grant-in-aid for Scientific Research from the Ministry of Education, Culture, Sports, Science, and Technology, Japan, by the National science foundation of China, and by the MOE ATU Program of R.O.C. NSC952112M009048. BR acknowledges the support of the Albert Einstein Minerva Center for Theoretical Physics and EZ the US-Israel Binational Science Foundation (BSF).

* Electronic address: haim.beidenkopf@weizmann.ac.il

- [1] D. Ertas and D.R. Nelson, *Physica C* **272**, 79 (1996).
- [2] G.P. Mikitik and E.H. Brandt, *Phys. Rev. B* **68**, 054509 (2003).
- [3] J. Kierfeld and V. Vinokur, *Phys. Rev. B* **69**, 024501 (2004).
- [4] V. Vinokur *et al.*, *Physica C* **295**, 209 (1998).
- [5] T. Giamarchi and P. LeDoussal, *Phys. Rev. B* **55**, 6577 (1997).
- [6] L.I. Glazman and A.E. Koshelev, *Phys. Rev. B* **43**, 2835 (1991).
- [7] M. Willemin *et al.*, *Phys. Rev. Lett.* **81**, 4236 (1998).
- [8] N. Avraham *et al.*, *Nature* **411**, 451 (2001).
- [9] H. Beidenkopf *et al.*, *Phys. Rev. Lett.* **95**, 257004 (2005).
- [10] S. Ooi, T. Shibauchi, and T. Tamegai, *Physica C* **302**, 339 (1998).
- [11] N. Motohira *et al.*, *J. Ceram. Soc. Jpn. Int. Ed.* **97**, 994 (1989).
- [12] G.C. Kim *et al.*, *Phys. Rev. B* **72**, 064525 (2005).
- [13] E. Zeldov *et al.*, *Nature* **375**, 373 (1995).
- [14] B. Khaykovich *et al.*, *Phys. Rev. B* **56**, R517 (1997).
- [15] Y. Radzyner, A. Shaulov, and Y. Yeshurun, *Phys. Rev. B* **65**, 100513(R) (2002).
- [16] P. Olsson and S. Teitel, *Phys. Rev. Lett.* **87**, 137001 (2001).
- [17] R. Cubitt *et al.*, *Nature* **365**, 407 (1993).
- [18] E. Zeldov *et al.*, *Europhys. Lett.* **30**, 367 (1995).
- [19] M. Konczykowski *et al.*, *Physica C* **332**, 219 (2000).
- [20] M.B. Gaifullin *et al.*, *Phys. Rev. Lett.* **84**, 2945 (2000).
- [21] F. Portier *et al.*, *Phys. Rev. B* **66**, 140511(R) (2002).
- [22] Y. Nonomura and X. Hu, *Phys. Rev. Lett.* **86**, 5140 (2001).
- [23] S. Ryu, A. Kapitulnik, and S. Doniach, *Phys. Rev. Lett.* **77**, 2300 (1996).
- [24] J.P. Rodriguez, *Phys. Rev. B* **73**, 214520 (2006).
- [25] D.T. Fuchs *et al.*, *Phys. Rev. Lett.* **80**, 4971 (1998).
- [26] C.D. Dewhurst and R.A. Doyle, *Phys. Rev. B* **56**, 10832 (1997).
- [27] Y. Matsuda *et al.*, *Phys. Rev. Lett.* **78**, 1972 (1997).
- [28] S. Ooi, T. Mochiku, and K. Hirata, *Physica C* **378**, 523

- (2002).
- [29] R. Sugano *et al.*, *Physica C* **388**, 637 (2003).
- [30] Y. Yamaguchi *et al.*, *Phys. Rev. B* **63**, 014504 (2000).
- [31] B. Khaykovich *et al.*, *Phys. Rev. Lett.* **76**, 2555 (1996).
- [32] T. Hanaguri *et al.*, *Physica C* **256**, 111 (1996).
- [33] G. Blatter, V.B. Geshkenbein, and A.I. Larkin, *Phys. Rev. Lett.* **68**, 875 (1992).
- [34] R.A. Klemm and J.R. Clem, *Phys. Rev. B* **21**, 1868 (1980).
- [35] L.L. Daemen *et al.*, *Phys. Rev. Lett.* **70**, 1167 (1993).
- [36] M. Tokunaga *et al.*, *Phys. Rev. B* **67**, 134501 (2003).
- [37] D. Li, B. Rosenstein, and V. Vinokur, *J. Supercond. Novel Mag.* **19**, 369 (2007).
- [38] D. Li and B. Rosenstein, *Phys. Rev. Lett.* **90**, 167004 (2003).
- [39] A.I. Larkin, and A. Varlamov. *Theory of fluctuations in superconductors* (Oxford, England, 2005), Chap. 2.
- [40] T.W. Li *et al.*, *Physica C* **257**, 179 (1996).